minerals

MDPI

Article

Experimental Study on Strengthening Carbothermic Reduction of Vanadium-Titanium-Magnetite by Adding CaF_2

Xiangdong Xing [1,2], Yueli Du [1], Jianlu Zheng [1], Yunfei Chen [3], Shan Ren [4,*] and Jiantao Ju [1,2,*]

1 School of Metallurgical Engineering, Xi'an University of Architecture and Technology, Xi'an 710055, China; xaxingxiangdong@163.com (X.X.); 18821795206@163.com (Y.D.); zhengjianlud@163.com (J.Z.)
2 Research Center of Metallurgical Engineering and Technology of Shaan Xi, Xi'an University of Architecture and Technology, Xi'an 710055, China
3 State Key Laboratory of Advanced Metallurgy, University of Science and Technology Beijing, Beijing 100083, China; b20180550@xs.ustb.edu.cn
4 College of Materials Science and Engineering, Chongqing University, Chongqing 400044, China
* Correspondence: shan.ren@cqu.edu.cn (S.R.); xaxxd@xauat.edu.cn (J.J.)

Received: 4 January 2020; Accepted: 24 February 2020; Published: 28 February 2020



Abstract: The effects and reduction mechanisms of carbothermic reduction of vanadium–titanium–magnetite were studied by adding various mass fractions of CaF_2 ranging from 0%, 1%, 3%, 5% to 7%. The results showed that the proper CaF_2 addition could strengthen the carbothermic reduction of vanadium–titanium–magnetite while the excessive amounts will weaken the promotive effect, hence the appropriate dosage was determined to be 3 mass%. The CaF_2 was favorable for the carbon gasification reaction, where it increased the partial pressure of CO inside briquette and caused the lattice distortion of vanadium–titanium–magnetite. The reaction improved the reduction process and accelerated the reduction rate. The appearance of $3CaO{\cdot}2SiO_2{\cdot}CaF_2$ and other complex compounds with low melting point facilitated the aggregation and growth of the slag and the iron, which increased the concentration of iron grains and the aggregation level of the slag.

Keywords: carbothermic reduction; calcium fluoride; vanadium–titanium–magnetite

1. Introduction

Vanadium–titanium–magnetite is a valuable resource [1–6]. Vanadium–titanium–magnetite has a variety of species, good conditions for storage, and high comprehensive utilization value. Vanadium–titanium–magnetite refining could recover a variety of valuable metal elements and obtain a variety of industrial products, which plays an important role in the metallurgical industry. The main refining technique for vanadium titanium magnetite is the "blast furnace-converter" process [7,8], which is limited by the fact that titanium is completely unrecoverable, it causes a huge waste of titanium resources and simultaneously environmental pollution. To realize the efficient utilization of vanadium–titanium–magnetite has been an industrial goal of related fields at home and abroad [9–12]. Solid-state reduction technology could get a better reduction effect at a lower temperature. However, due to the combination of different titanium compounds and iron compounds in vanadium–titanium–magnetite, the complex and dense mineral structure are formed, which makes reduction difficult [13,14]. Compared with the reduction of common iron-bearing minerals, vanadium–titanium–magnetite needs higher energy and lower production efficiency.

At present, there are a lot of previous researches regarding the reinforced carbothermic reduction of ilmenite [15–17]. However, few researches can be found regarding–vanadium titanium–magnetite. Song et al. [15] studied the carbothermic reduction process of ilmenite concentrates with added

sodium borate, demonstrating it can effectively improve the metallization degree of the carbothermic reduction and reduce the reduction temperature. Liu et al [16] investigated the effects of alkali metal additives on the pre-oxidation and the solid-state reduction reaction of ilmenite, indicating that many additives could promote the reaction. Borax ($Na_2B_4O_7$) was found to have an especially strong effect on the degree of reduction and metallization. Wu et al [17] discovered that alkali oxides could accelerate reduction reaction. Mono-metal oxide is better than binary, ternary, or quaternary oxides. Different alkali compounds as an accelerator could increase the metallization rate in different degrees [18]. Chen et al. [19] studied the various influencing factors of carbothermal reduction of vanadium–titanium–magnetite, and analyzed the reasons for the difficulty of reduction of vanadium–titanium–magnetite. The research on ilmenite reduction provided a lot of important information for the reinforced carbothermic reduction of vanadium–titanium–magnetite. The measure of adding catalysts is simple in operation, and the strengthening effect is obvious. CaF_2 is a flux commonly used in the metallurgical industry [20,21]. It is used in titanium-containing blast furnace slag, which reduces the viscosity and improves the stability. In addition, CaF_2 could be used not only as a reducing agent, but also as a carbon activation agent to make the carbon porous and subsequently more reactive. However, the effect of additives CaF_2 on vanadium titanium magnetite is not clear.

In the present study, the effect of adding CaF_2 on the isothermal carbothermal reduction process of vanadium–titanium–magnetite was studied. Meanwhile, the reduction mechanism was also studied using X-ray diffraction (XRD), scanning electron microscopy (SEM) and energy dispersive spectroscopy (EDS) to provide empirical guidance for the high efficient industrial utilization of the vanadium–titanium–magnetite.

2. Experiments

2.1. Experimental Materials

The material of vanadium–titanium–magnetite used in the current study was obtained from Liaoning, China. The ore was ground into fines with a size distribution of 98% less than 74 μm. Its component analysis and phase analysis are shown in Table 1 and Figure 1, respectively. The additive was analytic pure CaF_2 with a size distribution of 100% less than 74 μm. The reductant was high purity graphite powder with 99.8% fixed carbon.

Table 1. The compositions of the magnetite ore (mass percent, %).

FeO	Fe_2O_3	V_2O_5	TiO_2	SiO_2	Al_2O_3	CaO	MgO
20.60	51.27	1.85	12.96	6.28	1.74	3.72	0.29

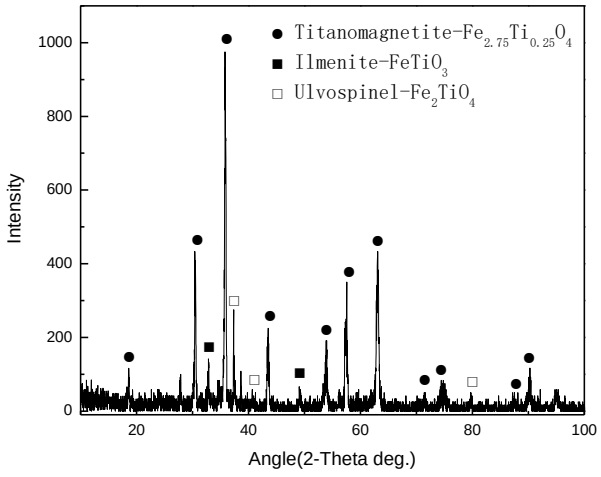


Figure 1. The X-ray diffraction (XRD) pattern of the vanadium–titanium–magnetite.

As shown in Table 1, the iron grade of vanadium–titanium–magnetite is relatively low and the MgO content is only 0.29%. The impurity content is high. The contents of SiO_2, Al_2O_3, and CaO are 6.28%, 1.74%, and 3.72% respectively. The TiO_2 content reaches 12.96%, which is difficult to utilize by traditional ironmaking technology. Figure 1 depicts the diffraction peaks of vanadium–titanium–magnetite concentrates, where the ores with superior crystallization are predominantly composed of iron, ilmenite ($FeTiO_3$), ulvospinel (Fe_2TiO_4) and titanomagnetite ($Fe_{2.75}Ti_{0.25}O_4$).

2.2. Experimental Process and Characterization Method

The main apparatus used for the experiment included a vacuum drying oven (DZF-6050), a molding press, a resistance furnace with a rated temperature of 1600 °C, an electronic balance, a data acquisition system, a thermocouple, and a temperature controller. The schematic diagram of the experimental apparatus is shown in Figure 2.

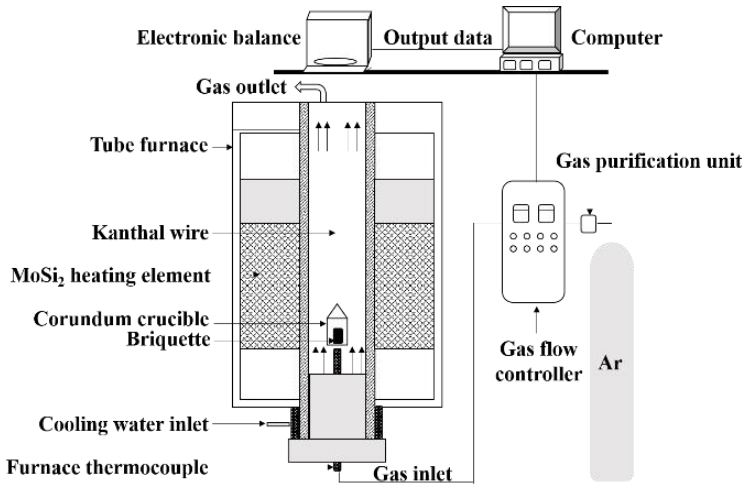


Figure 2. The schematic diagram of the experimental apparatus.

The isothermal experiment was used to clarify the mechanism that CaF_2 had on the carbothermic reduction process of vanadium–titanium–magnetite. The C/O was 1.2, and a certain amount of vanadium–titanium–magnetite and high purity graphite powder were weighed. The CaF_2 was added as 0%, 1%, 3%, 5%, and 7%.The powders were mixed homogeneously in acetone. The cylindrical samples were φ10 mm × 10 mm created via a molding press under 10 Mpa. The samples were dried for 2 h in a vacuum drying oven, and then loaded in the high-temperature experiment apparatus to conduct the isothermal reduction experiment. The experiments were finished at 1100 °C, 1200 °C, 1300 °C and 1400 °C, respectively. The exhaust gas was introduced into a container containing NaOH solution for the treatment of SiF_4. After the samples were kept at the experimental temperature, they were rapidly cooled in argon and analyzed via XRD and SEM-EDS. To characterize the effect of CaF_2 on the reduction process, the reaction fraction was selected as the evaluation index, seen in Equation (1).

$$f = \frac{\Delta W_t}{\Delta W\text{max}} \times 100\% \text{ ;} \quad (1)$$

f——reaction fraction, %;

$\triangle W_t$——the weight loss of the carbonaceous briquettes after the reduction time (t), g;

$\triangle W_{max}$——the maximum weight loss of the carbonaceous briquettes, g.

3. Results and Discussion

3.1. The Thermodynamic Analysis of Carbothermic Reduction

The carbothermic reduction process of vanadium–titanium–magnetite could be divided into two parts [22,23]. One part is that the iron oxides are directly reduced by C, the other is the indirect reduction which used CO as the reductant, containing carbon dissolution reaction as well as the reduction of iron compounds. The possible reactions are listed in Table 2. Figure 3 shows the relationship between the △G and the temperature.

Table 2. The main reactions during the reduction process.

Reaction Equation	Gibbs Free Energy (△G)/kJ bs fre	Temperature Range /°C	Equation
$2FeTiO_3 + C = FeTi_2O_5 + Fe + CO$	106.59 − 21.864T	400–1400	(2)
$FeTi_2O_5 + C = 2TiO_2 + Fe + CO$	101.06 − 42.408T	400–1400	(3)
$Fe_2TiO_4 + C = FeTiO_3 + Fe + CO$	88.607 − 0.0268T 3.8712 + 0.0478T	400–800 800–1400	(4)
$FeO + C = Fe + CO$	151.78 − 0.1529T	400–1400	(5)
$C + CO_2 = 2CO$	169.39 − 0.1738T	400–1400	(6)
$Fe_2TiO_4 + CO = FeTiO_3 + Fe + CO_2$	−9.5332 + 18.816T	400–1400	(7)
$2FeTiO_3 + CO = FeTi_2O_5 + Fe + CO_2$	43.199 − 0.0225T 48.709 − 0.0563T	400–700 700–1400	(8)
$FeTi_2O_5 + CO = 2TiO_2 + Fe + CO_2$	174.74 − 0.2503T	400–1400	(9)
$FeTiO_3 + CO = TiO_2 + Fe + CO_2$	118.63 − 0.1476T	400–1400	(10)
$3TiO_2 + CO = Ti_3O_5 + CO_2$	107.4 − 0.0263T	400–1400	(11)
$FeO + CO = Fe + CO_2$	−5.6599 + 2.0844T	400–1400	(12)
$3TiO_2 + C = Ti_3O_5 + CO$	273.595 − 0.1981T	400–1400	(13)
$TiO_2 + 3C = TiC + 2CO$	527.685 − 0.3367T	400–1400	(14)
$Ti_3O_5 + 3C = 3TiC + 2.5O_2$	590.396 − 0.1914T	400–700	(15)
$SiO_2 + C = SiO + CO$	668.07 − 0.3288T	400–1400	(16)
$SiO_2 + CO = SiO + CO_2$	505.76 − 0.1598T	400–800	(17)
$SiO + 3CO = SiC + 2CO_2$	−403.51 + 0.339T	400–1400	(18)
$SiO + 2C = SiC + CO$	−78.89 + 0.0010T	400–1400	(19)

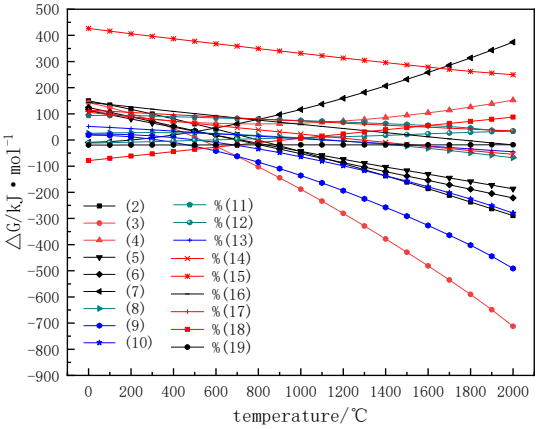


Figure 3. The relationship between the △G and the temperature.

Table 2 shows that these reactions are mainly endothermic. So it is favorable for improving reactions at high temperature. At the early stage, the low CO partial pressure inside briquette causes the reduction process to be primarily the solid-solid reaction between carbon and iron compounds. As the temperature increases, ferrotitanium compound reacts with CO easily.

3.2. Influence of Additive Amounts of CaF_2

The experiments were performed at various conditions, with 0%, 1%, 3%, 5%, and 7% CaF_2 in order to explore the influence of CaF_2 on the carbothermic reduction process. The results are shown in Figure 4.

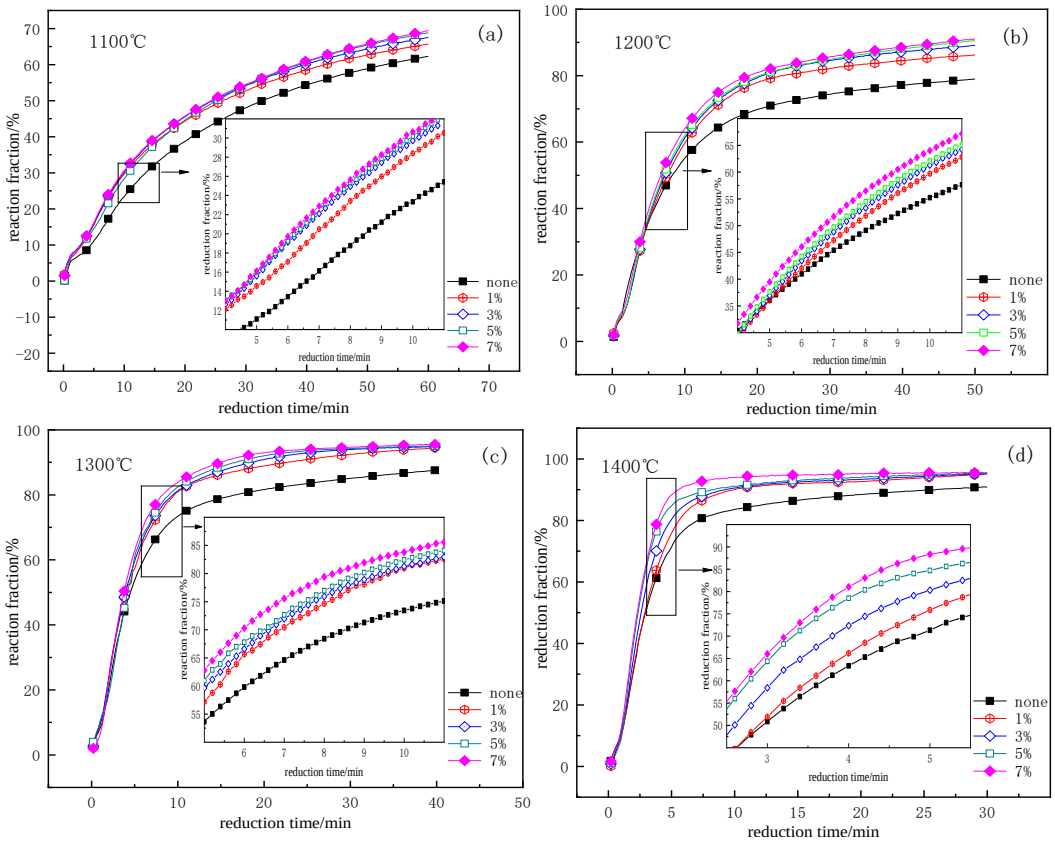


Figure 4. The relationship between the CaF_2 content and the reaction fraction (**a**). 1100 °C; (**b**). 1200 °C; (**c**). 1300 °C; (**d**). 1400 °C).

Figure 4 shows that the addition of CaF_2 can accelerate the reduction process. When the reduction temperature was 1100 °C, the reaction fraction rose by prolonging the reduction time, although the reaction could not reach equilibrium within the scope of the experiment time. The reaction process increased as the additive content increased and the temperature reduced with 1% CaF_2. The reaction process reduced when more than 3% CaF_2 was added. The higher the reduction temperature, the less time required for reduction equilibrium. When CaF_2 of 3% was added, the equilibrium time for the carbothermic reduction at 1200 °C, 1300 °C, and 1400 °C was 22 min, 10 min, and 6 min, respectively. The reaction fraction was close to 90% when 3% of the CaF_2 was added at 1200 °C. When the temperature was over 1300 °C, the change of reduction fraction was relatively small, reaching about 95% at 1400 °C. When CaF_2 of 7% was added, the reaction fraction increased, but the increasing trend was not obvious. The optimum conditions were obtained at the reduction temperature of 1300 °C and additive amounts of 3%.

3.3. Morphological Analysis

The non-CaF_2 and the 3% CaF_2 were chosen for the experiments at 1300 °C. Figure 5 shows the SEM-EDS results for the products obtained with a reduction time of 5 min, 10 min, 20 min, and 30 min, respectively.

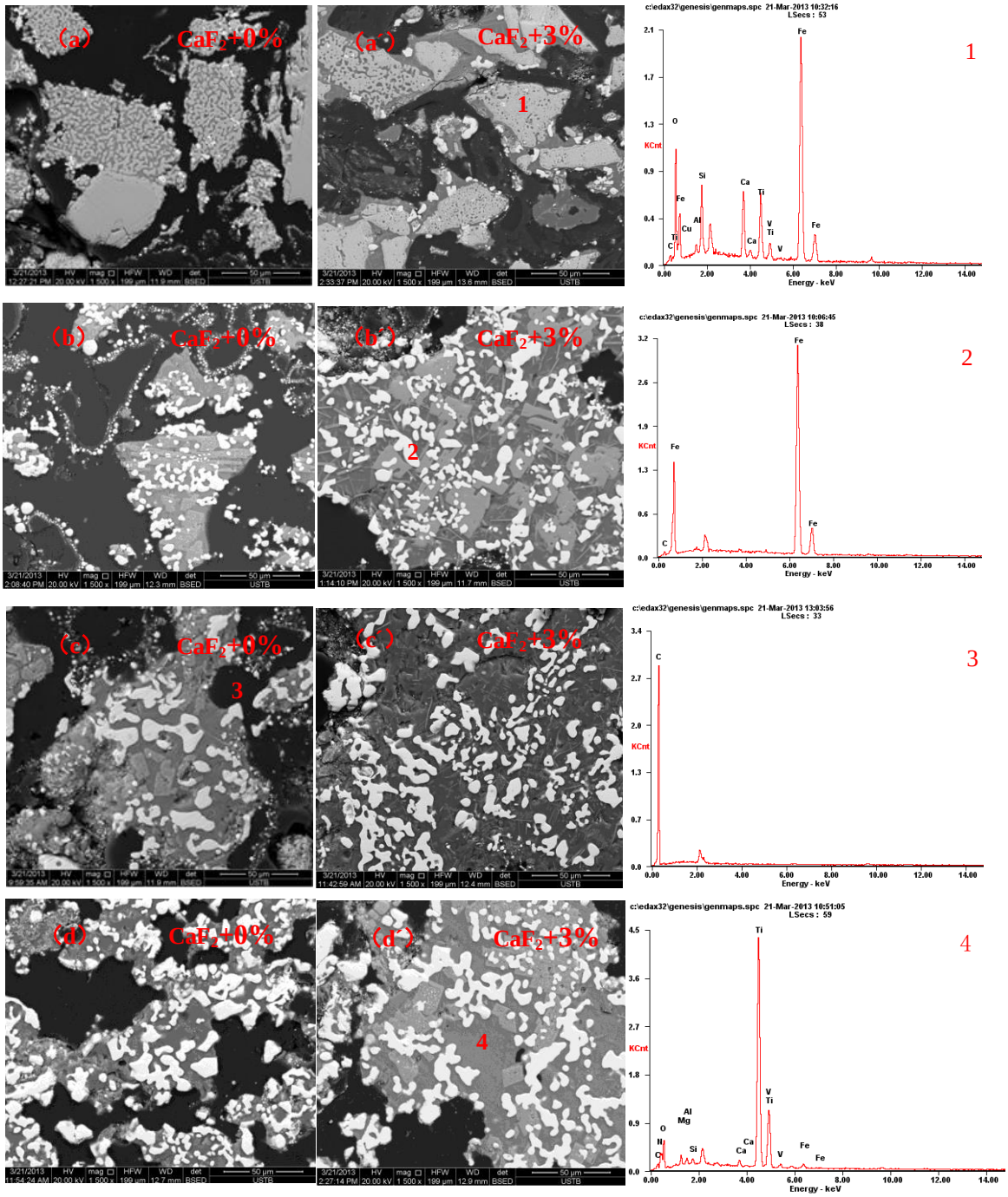


Figure 5. Scanning electron microscopy (SEM)- energy dispersive spectroscopy (EDS) analysis under various reduction time of (**a**) and (**a´**) 5 min, (**b**) and (**b´**) 10 min, (**c**) and (**c´**) 20 min, (**d**) and (**d´**) 30 min.

Figure 5 shows that the two types of samples could participate internally in the reduction reaction to generate bits of metallic iron quickly. The vanadium–titanium–magnetite particles reacted rapidly with the surrounding carbon and the CO created by the reaction. The particles were eroded gradually from outside to inside and the interface tended to be smooth. The iron grain size in the inner section of the reduction product with 3% CaF_2 was larger. Due to the erosion of CaF_2 and the occurrence of the reduction reaction, the surface of internal particles was relatively rough. As the reduction time increased, the iron phase inside samples increased constantly, and the grain size increased. However, the content or grain size of the iron phase inside briquettes adding CaF_2 was better than others. This phenomenon demonstrated that CaF_2 could enhance the chemical reaction rate. The larger the

partial pressure of CO, the faster the diffusion rate was into the particles to seize the oxygen bound to the iron. This suggested that CaF_2 expedited the Boudouard reaction to accelerate the CO generation rate, which raised the partial pressure of reducing gas. When the reduction time was 30 min, there were a large number of metal irons in the products with either none or 3% CaF_2. The mineral segregation results in a homogeneous distribution of metal iron around or inside the non-ferrous particles. The CaF_2 could not only facilitate the segregation of metal iron grains, but also erode the surface of particles to make them rough.

The grain sizes of the metal iron varied with the reduction time and they were analyzed with "Image-Pro-Plus", all the complete grains in the picture are selected out, and the average grain size is calculated. The results were shown in Figure 6. The CaF_2 had a significant effect on the formation, aggregation, and growth of the metal iron grains, and the effect was more evident with longer reduction time.

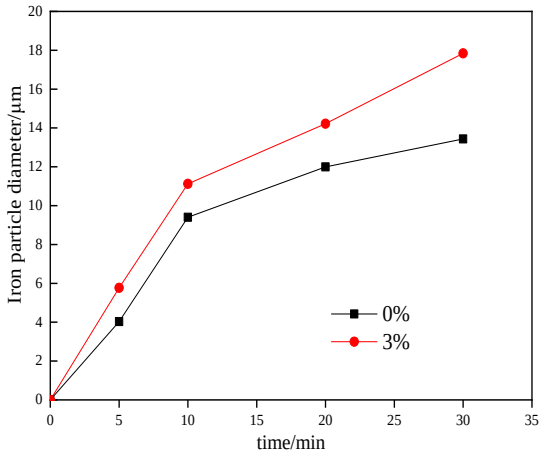


Figure 6. The effect of CaF_2 on the iron grain size in the reduction process.

3.4. XRD Analysis

Figure 7 shows the XRD results of the reduction products that were reacted with none or 3% CaF_2 for 5 min, 10 min, 20 min, and 30 min.

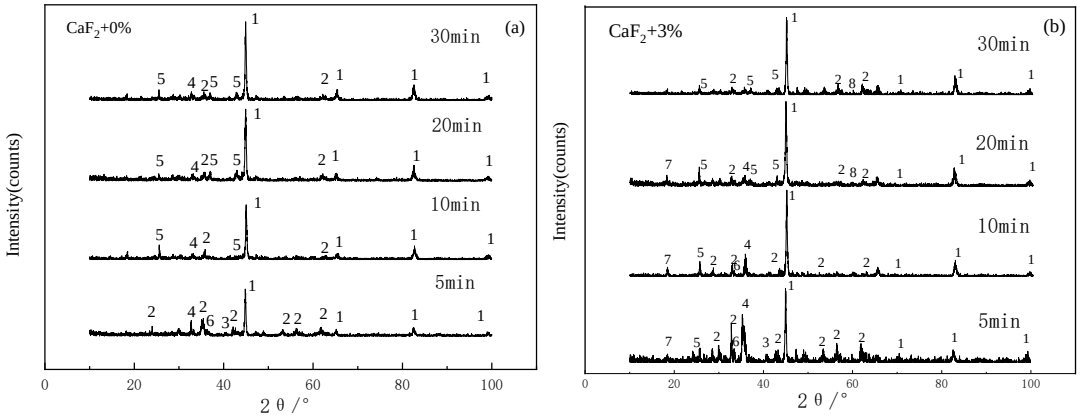


Figure 7. XRD patterns of the reduction products of (**a**) 0% CaF_2 and (**b**) 3% CaF_2 (1.Fe; 2.TTM; 3.FeO; 4.$FeTiO_3$; 5.$FeTi_2O_5$; 6.Fe_2TiO_4; 7.CaF_2; 8.$Ca_4Si_2F_2O_7$).

The principal phases (shown in Figure 7) were Fe, $FeTiO_3$, TTM, some Fe_2TiO_4 and $FeTi_2O_5$ after 5 min. The additive could be detected from the samples of 3% CaF_2, indicating that the CaF_2 did not react, basically remaining at the earlier stage. When the reduction time was 10 min, the CaF_2 did not change the product phases. The peak values of Fe and $FeTiO_3$ were high. The reaction time

extended and the CaF_2 with mixed mineral compositions including CaO and SiO_2 were in the reaction. $3CaO{\cdot}2SiO_2{\cdot}CaF_2$ is a low-melting complex compound, appeared, which was favorable for diffusion and iron phases aggregation. The production phases consisted of Fe, $FeTi_2O_5$ and a slight amount of titanomagnetite (TTM) with a 30 min reaction time. The behavior of the main phases in the reduction process is shown in Figure 8.

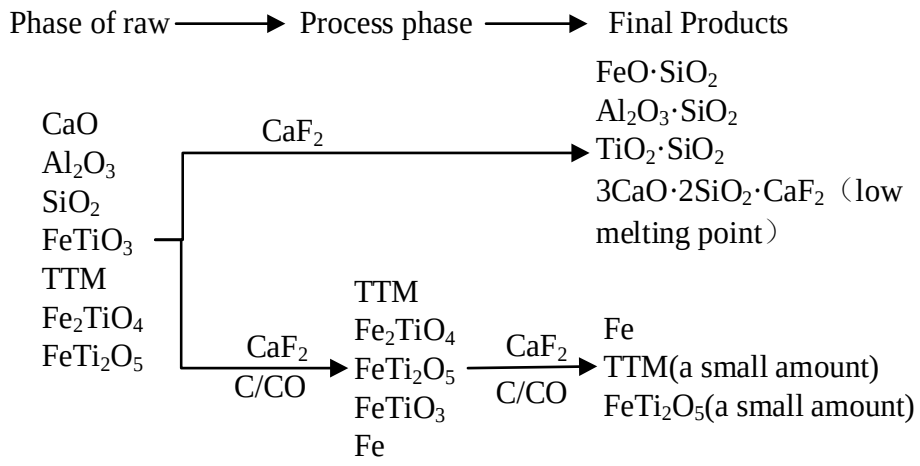


Figure 8. The schematic diagram of the main phase transformation.

The "Jade" software (Version 6.5) was used to interpret the XRD data of the 20 min reaction time in Figure 8. The XRD data of the crystal lattice parameters of the main phases amended by the "Rietveld" methods [21] are listed in Table 3.

Table 3. The crystal lattice parameters of the main phases.

Crystal Lattice Parameters	TTM		$FeTiO_3$		$FeTi_2O_5$		Fe_2TiO_4	
	0%CaF_2	3%CaF_2	0%CaF_2	3%CaF_2	0%CaF_2	3%CaF_2	0%CaF_2	3%CaF_2
a/Å	5.07824	5.07623	5.07934	5.07951	3.76023	3.75751	8.49324	8.50731
±	0.0001	0.0002	0.0002	0.0001	0.0002	0.0001	0.0002	0.0003
b/Å	-	-	-	-	9.65635	9.65635	-	-
±				0.0001	0.0003			
c/Å	13.43312	13.45201	-	-	9.98301	9.98190	-	-
±	0.0002	0.0001		0.0002	0.0001			
Volume/$Å^3$	346.42	346.63	131.04	131.06	362.27	363.36	612.66	615.71

Table 3 shows that the CaF_2 had particular influences on the crystal structure of the ferrotitanium phase contained in vanadium–titanium–magnetite during the reduction process. In the TTM phase, the crystal cell stretched along the axis c, decreased slightly along the axis a, and its volume expanded. The crystal lattice parameter shortened from 5.07824Å to 5.07623Å, value c increased from 13.43312Å to 13.45201Å, and volume expanded from 346.42$Å^3$ to 346.63$Å^3$. It can be observed that the change rules of the crystal lattice parameter of $FeTiO_3$, $FeTi_2O_5$ and Fe_2TiO_4 are similar. The CaF_2 distorted the crystal structure, which benefited the transformation of the TTM phase from the rhombohedral system to other reduction product crystal system and lowered the reduction difficulty between iron compounds with C and CO.

3.5. Mechanism Analysis of CaF_2

According to the analysis results depicted in Figure 5, Figure 7 and Table 3, the schematic diagram of the samples reduction process with adding CaF_2 is given in Figure 9. The CaF_2 had little effect on the reduction process at the initial stage. As the reaction layer thickened, the reduction degree of vanadium–titanium–magnetite rose, the iron grains proliferated, and the slag phase formed. The CaF_2

reacted with the high-melting-point phase to generate a certain amount of $3CaO{\cdot}2SiO_2{\cdot}CaF_2$, which had a low-melting-point and could be a "lubricant" to the reaction layer and the interstitial flow, promoting the migration of the iron and the aggregation of slag.

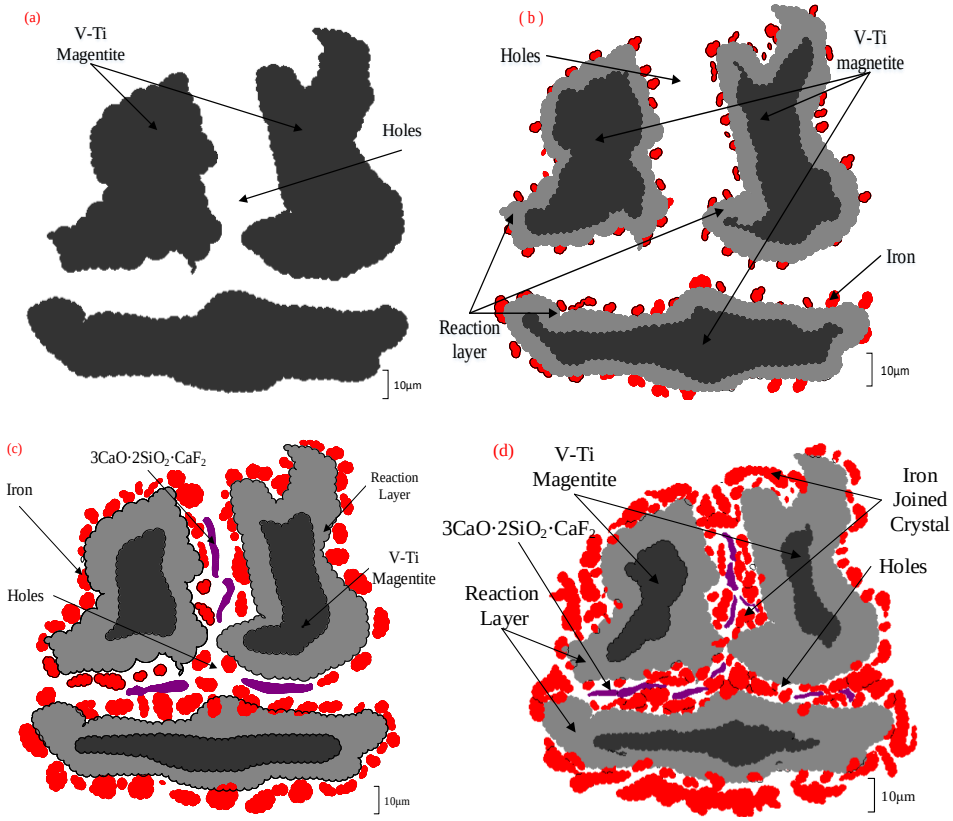


Figure 9. The action mechanism of the CaF_2 (**a**). initial sample; (**b**). early reaction; (**c**). middle reaction; (**d**). end reaction).

Vanadium–titanium–magnetite with the CaF_2 enabled the equilibrium of the original Boudouard reaction to be broken and then to catalytically form a new one, seen in Equations (20) and (22).

$$2CaF_2 + 2C + SiO_2 = 2Ca(g) + SiF_4(g) + 2CO(g) \quad (20)$$

$$Ca(g) + 4CO(g) = CaC_2 + 2CO_2(g) \quad (21)$$

$$2CaC_2 + SiF_4(g) + 6CO_2(g) = 2CaF_2 + SiO_2 + 10CO(g). \quad (22)$$

The favorable reaction activity of the Ca (g) was not the restrictive step of the reaction, but rather led to its higher reaction rate. Equations (21) and (22) were combined to form the catalytic reaction cycle, which sped up the Boudouard reaction and produced CO, which improved the reduction process of the ferrotitanium compounds. The carbon surface participated in the Boudouard reaction that intensified the surface erosion degree of the high purity graphite powder. The larger contact area between the carbon particles and the vanadium–titanium–magnetite would update carbon layers to pile up the active points into the carbon surface and to build up the solid-solid reduction.

4. Conclusions

The addition of CaF_2 facilitated the carbothermic reduction of the vanadium–titanium–magnetite, enhanced the reaction fraction, and the continuously increasing additive amounts and reduction

temperature led to the reaction fraction tending to increase slowly. The appropriate condition was 3% CaF_2 at 1300 °C, where reaction fraction could reach up to 95%.

The CaF_2 accelerated the diffusion and migration of the metal iron points, extended the grain size, eroded the surface of the vanadium–titanium–magnetite particles, destroyed the crystal structure of the non-metallic reduction products in the specimens, promoted the aggregation of the particles like titanomagnetite, ilmenite, and ferrous brookite, increased the lattice distortion of the reduced phase, and improved the reduction capacity.

Vanadium–titanium–magnetite with CaF_2 disrupted the equilibrium of the original Boudouard reaction which formed a new catalytic reaction, and the larger contact area between the carbon particles and the vanadium–titanium–magnetite updated the carbon layers to pile up the active points in the carbon surface.

Author Contributions: Conceptualization, X.X. and Y.D.; methodology, X.X. and Y.D.; software, Y.D. and J.Z.; validation, Y.D., J.Z and Y.C.; formal analysis, S.R. and J.J.; investigation, X.X.; resources, S.R. and J.J.; data curation, X.X. and Y.D.; writing—original draft preparation, X.X. and Y.D.; writing—review and editing, X.X.; supervision, S.R. and J.J.; project administration, X.X.; funding acquisition, X.X. All authors have read and agreed to the published version of the manuscript.

Funding: The present work was financed by National Nature Science Foundation of China (Grant No. 51604209) and the Natural Science Basic Research Program of Shaanxi (Program No. 2019JLP-05).

Conflicts of Interest: The authors declare no conflict of interest.

References

1. Huang, R.; Lv, X.; Bai, C.; Zhang, K.; Qiu, G.B. Enhancement reduction of Panzhihua ilmenite concentrate with coke and conglomeration of metal with ferrosilicon. *Steel Res. Int.* **2013**, *84*, 892–898. [CrossRef]
2. Pesl, J.; Eric, R.H. High temperature carbothermic reduction of Fe_2O_3-TiO_2-M_xO_y oxide mixtures. *Miner. Eng.* **2002**, *15*, 971–984. [CrossRef]
3. Xing, X.D.; Wang, S.; Pang, Z.G.; Zhang, Q.L. Effect of B_2O_3 on the carbothermal reduction of vanadium titanium magnetite. *Metall. Res. Technol.* **2019**, *116*, 630.
4. Jiang, T.; Xu, J.; Guan, S.F.; Xue, X.-X. Study on coal-based direct reduction of high-chromium vanadium-titanium magnetite. *Northeast. Univ.* **2015**, *85*, 77–80.
5. Cheng, G.J.; Xue, X.X.; Gao, Z.X.; Jiang, T.; Yang, H.; Duan, P.N. Effect of Cr_2O_3 on the reduction and smelting mechanism of high-chromium vanadium-titanium magnetite pellets. *ISIJ Int.* **2016**, *56*, 1938–1947. [CrossRef]
6. Lv, W.; Lv, X.W.; Xiang, J.Y.; Zhang, Y.Y.; Li, S.P.; Bai, C.G.; Song, B.; Han, K.X. A novel process to prepare high-titanium slag by carbothermic reduction of pre-oxidized ilmenite concentrate with the addition of Na_2SO_4. *Int. J. Miner. Process.* **2019**, *167*, 68–78. [CrossRef]
7. Xing, X.D.; Chen, Y.F.; Liu, Y.R. Study of the reduction mechanism of ironsands with addition of blast furnace bag dust. *Metall. Res. Technol.* **2018**, *115*, 214. [CrossRef]
8. Chen, D.S.; Song, B.; Wang, L.N.; Qi, T.; Wang, W.J. Direct reduction and enhanced reduction of vanadium-bearing titanomagnetite concentrates. *J. Univ. Sci.Technol. B* **2011**, *33*, 1331–1336.
9. Lv, X.W.; Lun, Z.G.; Yin, J.Q.; Bai, C.G. Carbothermic reduction of vanadium titanomagnetite by microwave irradiation and smelting behavior. *ISIJ Int.* **2013**, *53*, 1115–1119. [CrossRef]
10. Xing, X.D.; Pang, Z.G.; Mo, C.; Wang, S.; Ju, J.T. Effect of MgO and BaO on viscosity and structure of blast furnace slag. *J. Non-Cryst. Solids* **2020**, *530*, 119801. [CrossRef]
11. El-Tawil, S.Z.; Morsi, J.M.; Abdalla, F.H.A. Reductive roasting of pre-oxidized titanomagnetite ore. *Rare Metal* **1990**, *9*, 170–178.
12. Shi, L.Y.; Zhen, Y.L.; Chen, D.S.; Wang, L.N.; Qi, T. Carbothermic reduction of vanadium-titanium magnetite in molten NaOH. *ISIJ Int.* **2018**, *58*, 627–632. [CrossRef]
13. Xing, X.D.; Liu, Y.R.; Ju, J.T.; Liu, Z.J.; Liu, X.L.; Li, N.Y.; Shen, Y.S. Synthesis and non-isothermal carbothermic reduction of $FeTiO_3$-Fe_2O_3 solid solution systems. *Rare Metal Mater. Eng.* **2018**, *47*, 2775–2781.
14. Xing, X.D.; Wang, S.; Zhang, Q.L. Thermogravimetric analysis and kinetics of mixed combustion of waste plastics and semicoke. *J. Chem.* **2019**, *2019*, 8675986. [CrossRef]

15. Song, B.; Lv, X.W.; Miao, H.H.; Han, K.X.; Zhang, K.; Huang, R. Effect of $Na_2B_4O_7$ addition on carbothermic reduction of ilmenite concentrate. *ISIJ Int.* **2016**, *56*, 2140–2146. [CrossRef]
16. Liu, S.S.; Guo, Y.F.; Qiu, G.; Jiang, Z.; Chen, F. Solid-state reduction kinetics and mechanism of pre-oxidized vanadium-titanium magnetite concentrate. *Trans. Nonferrous Metals Soc.* **2014**, *24*, 3372–3377. [CrossRef]
17. Wu, J.H.; Sun, K.; Ma, Y.Y.; Liu, M.Y.; Zhang, Y. Catalytic effect of alkali chlorides on carbothermic reduction of pre oxidized ilmenite. *Trans. Nonferrous Metals Soc.* **2000**, *10*, 813–816.
18. Paktunc, D.; Thibault, Y.; Sokhanvaran, S.; Yu, D. Influences of alkali fluxes on direct reduction of chromite for ferrochrome production. *SAIMM* **2018**, *118*, 1305–1314. [CrossRef]
19. Chen, S.Y.; Fu, X.J.; Chu, M.S.; Li, X.Z.; Liu, Z.G.; Tang, J. Carbothermic reduction mechanism of vanadium-titanium magnetite. *J. Iron Steel Res. Int.* **2016**, *23*, 409–414. [CrossRef]
20. Cui, S.Q.; Lu, Q.; Feng, S.; Sun, Y.Q.; Chen, S.J.; Li, F.M.; Wan, X.Y.; Kang, Z.P. Research on effect of additives on viscosity of titanium-bearing blast furnace slag of Chengde steel. *Iron Steel Van. Titanium* **2014**, *35*, 68–72.
21. Yu, D.W.; Paktunc, D. Carbothermic reduction of chromite fluxed with aluminum spent potlining. *Trans. Nonferrous Metals Soc. China* **2019**, *29*, 200–212. [CrossRef]
22. Sun, H.Y.; Adetoro, A.A.; Wang, Z.; Pan, F.; Li, L. Direct reduction behaviors of titanomagnetite ore by carbon in fluidized bed. *ISIJ Int.* **2016**, *56*, 936–943. [CrossRef]
23. Wang, Z.Y.; Zhang, J.L.; Jiao, K.X.; Liu, Z.J.; Barati, M. Effect of pre-oxidation on the kinetics of reduction of ironsand. *J. Alloy Compd.* **2017**, *729*, 874–883. [CrossRef]



© 2020 by the authors. Licensee MDPI, Basel, Switzerland. This article is an open access article distributed under the terms and conditions of the Creative Commons Attribution (CC BY) license (http://creativecommons.org/licenses/by/4.0/).